New approach for particle size and shape analysis of iron-based oxygen carriers at different oxidation degrees

Particuology 90 (2024) 493–503

Contents lists available at ScienceDirect

Particuology

journal homepage: www.elsevier.com/locate/partic

New approach for particle size and shape analysis of iron-based oxygen carriers at multiple oxidation states

Victor Purnomo [a,*], Marcelo Dal Belo Takehara [b], Robin Faust [a], Lidiya Abdisa Ejjeta [a], Henrik Leion [a]

[a] Division of Energy and Materials, Department of Chemistry and Chemical Engineering, Chalmers University of Technology, Göteborg 412 58, Sweden
[b] Division of Energy Science, Department of Engineering Sciences and Mathematics, Luleå University of Technology, Luleå 971 87, Sweden

ARTICLE INFO

Article history:
Received 23 December 2023
Received in revised form
18 January 2024
Accepted 23 January 2024
Available online 1 February 2024

Keywords:
Oxygen carrier
Size and shape analysis
Dynamic image analysis
Oxidation state
Fluidized bed
Chemical looping

ABSTRACT

One of the crucial issues in the chemical looping technology lies in its bed material: the oxygen carrier. Particle size analysis of an oxygen carrier is important since in a fluidized bed the material can only work well within a specific size range. While the favorable size ranges for oxygen carrier materials have already been reported, none of the published studies has analyzed the particle size and shape of oxygen carriers in detail. Furthermore, the effect of oxygen carriers' oxidation degree on such properties has not been considered either. This study aimed to report the particle size and shape analysis of five iron-based oxygen carriers, one natural ore, one synthetic material, and three residue products, at different oxidation degrees using dynamic image analysis (DIA). The oxygen carriers were prepared at different mass conversion degrees in a fluidized bed batch reactor. The size distribution, sphericity, and aspect ratio of the oxygen carrier particles were examined experimentally using a Camsizer instrument. Our results show that the DIA method was successfully able to analyze the particle size and shape of our oxygen carriers with satisfying accuracy for comparison. The oxidation state of the investigated materials seems to only affect the particle size and shape of oxygen carriers to a minor extent. However, exposures to redox cycles in a fluidized bed reactor may alter the particle size and shape of most oxygen carriers.

1. Introduction

Oxygen carriers are promising bed materials that can be used in a wide range of technologies comprising one or more fluidized bed reactors. The material in its simplest form is usually a transition metal oxide, but it may also comprise a mixture of various metal oxides and possibly support materials. The most notable characteristic is its ability to undergo oxidation and reduction reactions multiple times at the conditions present in fluidized bed reactors. In a simple boiler, this trait has been proven to enhance the heat and oxygen distribution inside the combustion chamber (Ma et al., 2022), which also leads to a higher combustion efficiency compared to that when using quartz sand as the bed material. This innovation, known as oxygen carrier aided combustion (OCAC), has been run commercially and semi-commercially since 2012 in several sites in Sweden (Störner et al., 2021).

When it comes to a more advanced technology, the role of an oxygen carrier is essential in establishing a successful operation of chemical looping technology (Zheng et al., 2022). Comprising two fluidized bed reactors, a chemical looping unit involves separate oxidation–reduction reactions, which take place in air and fuel reactor, respectively. The oxygen carrier is circulated between both reactors to undergo oxidation in the air reactor (AR) and reduction, which implies a fuel conversion, in the fuel reactor (FR). In this way, it is possible to obtain a high-quality product gas stream without the presence of nitrogen, making the CO_2 capture much easier and even more efficient (Khan et al., 2020). Fig. 1 illustrates both OCAC and chemical looping combustion (CLC) (Hildor et al., 2022).

Many studies have been performed to characterize, screen, and examine various oxygen carrier materials for different purposes. Some reviews already summarized different iron-based oxygen carriers and their important properties, including the relevant challenges for the development of oxygen carriers (De Vos et al., 2020; Luo et al., 2015; Qasim et al., 2021; Yu et al., 2019). Adánez et al. (2004) presented several key criteria to screen an oxygen carrier, which include mechanical strength and reactivity. Lyngfelt

* Corresponding author.
E-mail address: purnomo@chalmers.se (V. Purnomo).

https://doi.org/10.1016/j.partic.2024.01.010

Nomenclature

A	Actual surface area of particles, μm^2
L	Particle length, μm
P	Perimeter of equivalent circle with the same surface area as the particles, μm
Ps	Actual perimeter of particles, μm
$x_{c,min}$	particle width/characteristic size, μm
$x_{Fe,max}$	Feret diameter, μm

Greek symbols

ω	Mass conversion degree
θ	Observation angle in XRD

Abbreviations

AR	Air reactor
CLC	Chemical looping combustion
DIA	Dynamic image analysis
FC	Freshly calcined
FO	Fully oxidized
FR	Fuel reactor
IL	Ilmenite ore
IS	Iron sand
LD	Linz-Donawitz
MR	Moderately reduced
MS	Mill scale
OCAC	Oxygen carrier aided combustion
SI	Synthetic ilmenite
SR	Substantially reduced

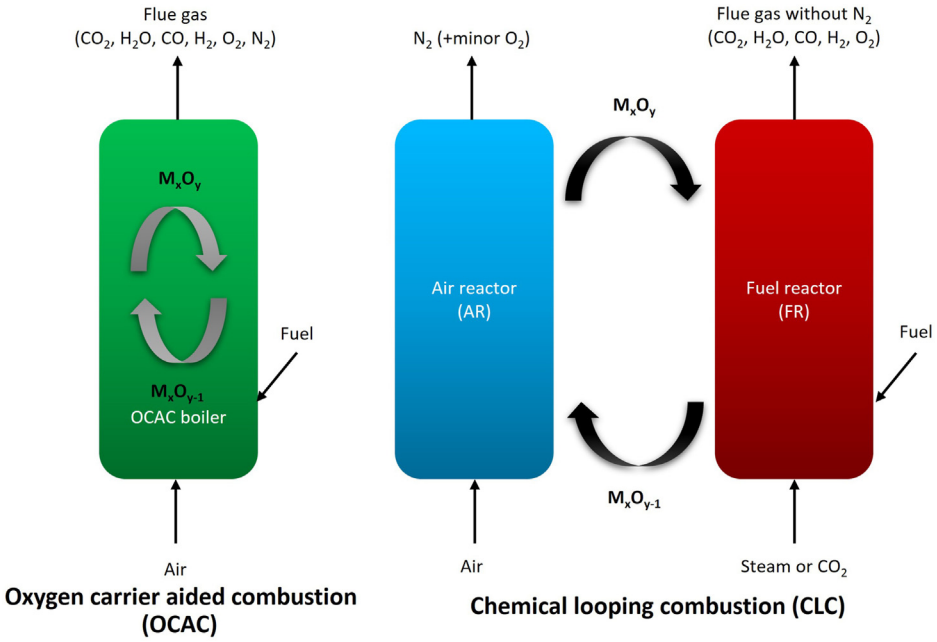

Fig. 1. Schematic diagrams of OCAC and CLC. M_xO_y and M_xO_{y-1} symbolize an oxidized and reduced oxygen carrier, respectively, and do not necessarily adhere to the real chemical formula.

(2011) reported the use of 700 different oxygen carrier materials in chemical looping combustion reactors at different capacity for a couple thousands of hours. Understandably, oxygen carrier's reactivity has become one the most addressed properties in the majority of the published works (Askaripour, 2018; Cuadrat et al., 2012; Ryu et al., 2003; Sedor et al., 2008). Oxidation state has been reported to be an important factor that may influence oxygen carrier's physical performance (Purnomo et al., 2021; Purnomo et al., submitted for publication). But the particle size and shape of oxygen carriers at different oxidation degrees have gained only a little interest.

In a fluidized bed setup of a chemical looping unit, an oxygen carrier may only work in a specific suitable size range (De Vos et al., 2020). The usual recommended size range for a chemical looping unit, including the currently largest chemical looping unit with a capacity of 1 MW in Germany, usually lies within 100–300 μm (Abián et al., 2017; Cho et al., 2004; Ding et al., 2018; Marx et al., 2021; Ryden et al., 2014; Zornoza et al., 2022). The oxygen carrying particles in an actual industrial process, including chemical looping, are usually not a perfect sphere (Hilton et al., 2010); even synthetically made particles can only be so close to spherical (Mattisson et al., 2014). Previous studies have reported that the shape of the bed particles influences both fluid dynamics and gas–solid hydrodynamics in a fluidized bed — being crucial to a chemical looping unit (Eppala et al., 2023; Ocanha et al., 2020). Mema et al. (2020) reported that a bed of elongated particles may lead to a more turbulent fluidization behavior compared to the one comprising spherical particles. Furthermore, particle morphology reportedly impacts the interactions between bed particles and ash compounds originating from solid fuels like biomass (Faust et al., 2023). These motivate the importance of performing a detailed particle size and shape analysis of the known oxygen carriers in the chemical looping research field.

Among different known methods for particle size and shape analysis, the dynamic image analysis (DIA) technique has been reported as a quick, efficient way to analyze particle size distribution (Takehara et al., 2022) and various particle shape parameters, including aspect ratio and sphericity (Li & Iskander, 2021). The method has been standardized and described in ISO 13322-2:2021 (International Organization for Standardization, 2021) — making it suitable for industrial applications. Several previous studies have utilized this standardized method for different purposes. For instance, Eggers et al. (2023) investigated the sphericity and aspect ratio of the sintering powder, Wei et al. (2022) investigated particle breakage and morphology changes of a type of sand, and Lunewski and Schmidt (2023) examined how elongated paper dust generated during a knife edge cutting was. But the method has never been previously used to investigate the particle size and shape of oxygen carriers, particularly for chemical looping applications and let alone at different oxidation states.

In this study, we performed particle size and shape analysis of five different iron-based oxygen carriers, comprising one synthetic, one natural, and three waste materials, using the DIA method. All the materials were prepared at three different oxidation degrees in a fluidized bed batch reactor. Furthermore, the crystalline phases of each sample were characterized and the effect of these on particle size and shape was analyzed. Our initial hypothesis was that different oxidation degrees lead to different phase composition, which can later affect the size and shape of the particles.

2. Materials and methods

2.1. Oxygen carriers

This work involves five different iron-based oxygen carriers. They are:

(i) Ilmenite ore, obtained from Titania A/S in Norway. This material is known as one of the benchmark oxygen carrier materials in chemical looping research fields due to its stable reactivity and robustness. The material consists of mostly oxides of iron and titanium.
(ii) Synthetic ilmenite, produced by CSIC in Spain from Fe_2O_3/TiO_2 precursors.
(iii) Iron sand, also known as copper slag, a by-product from the fuming process in copper production owned by Boliden AB in Sweden. Its main composition comprises iron and silicon oxides.
(iv) LD slag, also known as steel converter slag, a by-product from steel production owned by SSAB in Sweden. The material mostly consists of calcium and iron oxides.
(v) Mill scale, which is a steel rolled sheet residue, also obtained from SSAB. The material contains almost 100% iron oxides.

Apart from these oxygen carrier materials, quartz sand is also included in this study as reference due to its common use as bed material. The normalized oxygen-free composition and measured bulk density of the freshly calcined oxygen carriers is provided in Table 1 (Purnomo et al., 2023).

All these materials were calcined in a high-temperature furnace at (950 °C, 12 h) and then mechanically sieved to the 125–180 μm size range. At this state, the materials are at a fresh-calcined (FC) state. Twenty grams of each oxygen carrier were prepared in a fluidized bed batch reactor by exposing it to multiple redox cycles at 900 °C. Depending on the gas, the fluidization velocity ranged from 0.02 to 0.04 m/s, which corresponds to approximately 2–4 times the minimum fluidization velocity, respectively. These comprise:

Table 1
Oxygen-free elemental composition of the investigated iron-based oxygen carrier materials.

Oxygen carrier	Elemental composition (wt%)					Bulk density (kg/m^3)
	Fe	Mn	Ti	Si	Ca	
Ilmenite ore	54	0.7	45	0.2	0.1	2086
Synthetic ilmenite	54	–	46	–	–	1068
Iron sand	65	0.6	0.2	30	4.2	1398
LD slag	29.3	4.5	1.3	9.7	55.2	1197
Mill scale	95	1.0	–	4.0	–	2094

(i) Ten repeated redox cycles to stabilize the material reactivity, i.e., activate the material (Adánez et al., 2010). Here, the oxygen carrier sample was always completely oxidized before it got reduced with syngas (450 mL/min) for 20 s. An inert phase was introduced between each mentioned step to purge the remaining gas from the previous step.
(ii) The final eleventh cycle, where the oxygen carrier was reduced for a certain period, which leads to its final mass conversion degree (ω). These periods were determined based on our previous experiments on these materials, where the oxygen transfer capacity of the materials was estimated. The sample was then cooled down in an inert atmosphere.

The complete procedure in a single cycle is shown in Table 2 and the details of the fluidized bed setup have been published elsewhere (Leion et al., 2018).

A mass conversion degree value of 1 or 100 wt% indicates a fully oxidized (FO) state. Any value below this indicates that an oxygen carrier is partially oxidized or reduced, depending on the context. Since the last ω of the oxygen carriers in this study was set under a reduction cycle, the correct nomenclature should be a reduced oxygen carrier. The mass conversion degree of each oxygen carrier sample after this procedure is presented in Table 3. Note that the combination of the sample codes in this table are used in Section 3. For example, the sample code for freshly calcined ilmenite ore is ILFC. Also, note that the level of reduction is higher for the mill scale.

2.2. Particle size analysis

After the fluidized bed experiments, particle size analysis was performed on each oxygen carrier material using a particle size analyzer (Camsizer XT, Retsch GmbH, Germany), which is able to investigate powders and granules in a size range from 1 μm to 3 mm with dynamic image analysis (DIA). Note that the particles were sieved to 125–180 μm size range before the fluidized bed experiments. The particles were fed from a hopper by vibration and transported by a chute into the field of view. Here, the dispersed particles passed through a pair of LED light sources, which have different angles. Two different methods, namely air pressure dispersion (X-jet) and gravity dispersion (X-fall), were implemented and compared in this work to disperse the particles. The X-jet method was carried out with a dispersion pressure of 30 kPa. The principal differences between these methods are elaborated in Table 4.

The created shadows were subsequently captured by two high resolution cameras, one being responsible for small particles (zoom camera) while the other for the large particles (basic camera). These shadowgraph images were then processed for particle size and shape analysis by the Camsizer XT software (version 6.9.66.1206, Microtrac Retsch GmbH, Germany). This procedure was repeated 2–3 times for each oxygen carrier using at least 7–8 g sample. In case of limited amount, the repetition was performed using the

Table 2
Procedure in a single redox cycle performed in the fluidized bed batch reactor.

Step	Gas	Volumetric flow (mL/min)	Duration (s)	Note
Oxidation	5% O_2 in N_2	1000	Until the oxygen carrier becomes fully oxidized	Indicated by the outlet O_2 concentration returning to 5%
Inert	100% N_2	1000	180	
Reduction	50% CO in H_2 (syngas)	450	20	This duration only applies to cycle #1–#10. The eleventh cycle, which determines the final ω of the oxygen carrier, involves different durations depending on the oxygen transfer capacity of the materials.
Inert	100% N_2	1000	180	

Table 3
Mass conversion degree of the oxygen carrier samples.

Oxygen carriers	Freshly calcined (FC)	Fully oxidized (FO)	Moderately reduced (MR)	Substantially reduced (SR)
Ilmenite ore (IL)	1.00	1.00	0.99	0.98
Synthetic ilmenite (SI)	1.00	1.00	0.99	0.98
Iron sand (IS)	1.00	1.00	0.99	0.98
LD slag (LD)	1.00	1.00	0.99	0.98
Mill scale (MS)	1.00	1.00	0.96	0.91

Table 4
Comparison between two modular designs used for DIA of oxygen carrier particles.

Subject	Air pressure dispersion (X-jet)	Gravity dispersion (X-fall)
Technique	Dispersion using a compressed air through a venturi nozzle	Dispersion using the gravitational force
Measurement range (applicable particle size)	1 μm–1.5 mm	10 μm–3 mm
Advantages	Ability to break agglomerates	• Relatively simple • Sample can be easily recollected
Drawbacks	• Too much pressure may damage the primary particles • Sample recovery is only possible with an extra cyclone	May incur a larger measurement error in the presence of agglomerates

same batch of samples. Samples were divided homogeneously with a rotary divider (Retsch Technology, Germany).

2.3. Characterization

The crystalline phases of each oxygen carrier sample were characterized by using XRD D8 Discover with Mo K_α radiation ($\lambda = 0.70930$ Å) and measured within the 2θ range of 10°–55°. Mo K_α was used instead of the commonly applied Cu K_α to reduce sample fluorescence due to the presence of Fe in the samples. The SEM imaging of the cross-section of oxygen carriers (embedded in epoxy) was performed using a Phenom ProX SEM/EDX (Netherlands).

2.4. Data analysis

The size distribution can be characterized by different dimensions, such as equivalent particle diameter, particle width, and length. In this work, the particle width was selected to characterize the particle dimension, due to the good agreement with the sieving method. The particle width, $x_{c,min}$, is defined as the narrowest distance between two points on the particle edges among all the measured chords, perpendicular to the scanning direction. The opposite of this, i.e., the longest distance, is called the particle length, $x_{Fe,max}$, which is determined from the longest of all measured Feret diameters (maximum distance between two parallel tangents). Fig. 2 illustrates these measurements in a single particle.

Sphericity is the ratio of the perimeter of the equivalent circle P_s (based on the same surface area, A) to the actual perimeter P of the particle. This can be further expressed as follows.

$$\text{Sphericity} = \frac{P_s}{P} = \frac{\sqrt{4\pi A}}{P} \quad (1)$$

The aspect ratio of a particle is defined as the ratio between its width to its length.

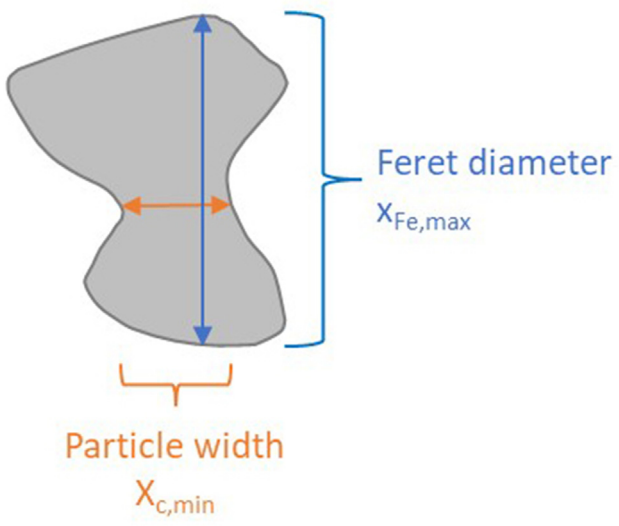

Fig. 2. Illustrations of particle width and Feret diameter in a single particle.

$$\text{Aspect ratio} = \frac{x_{c,min}}{x_{Fe,max}} \quad (2)$$

3. Results and discussion

3.1. Dispersion method comparison and weight losses during analysis

Both X-jet and X-fall methods were used to examine the freshly calcined ilmenite ore (ILFC) in two size ranges, i.e., 125–180 μm and 180–500 μm, and compared. The results illustrated in Fig. 3 show no significant difference between the two dispersion methods despite slight differences from the sieving results. This suggests that both methods work well for oxygen carrier particle size analysis. Since sample recovery was desired and our samples do not contain agglomerates, we decided to use the X-fall dispersion method for the rest of the samples.

When it comes to weight loss for the rest of the oxygen carrier samples during the particle shape and size analysis, the average weight loss is 0.7 wt%. Fig. 4 illustrates the weight loss of each oxygen carrier sample. Sand is included as reference.

Among all samples, LDFO and LDSR has shown the highest and second highest weight loss during the analysis. This may be attributed to the fact that LD slag has a complex composition of various minerals and, hence, may easily get fragmented — something which has been previously reported by Hildor et al. (2019). This information also agrees with the high number of fines presented in both samples, which is discussed in the next section. The fact that ILFC has had a higher loss than the other ilmenite ore samples may be due to this being the first sample to be investigated with this method, hence the trials and errors over three repetitions. Nevertheless, most samples lost less than 1.5 wt% of their weight and no sample lost more than 4 wt% of its original weight. This demonstrates that precise amounts and no contamination between samples were identified during the runs. This characteristic is very attractive considering the low amount of material and representability required to validate the method for the oxygen carrier materials. Over one million particles were detected by the software.

3.2. Particle size distribution at different mass conversion degrees

The particle width, i.e., characteristic size chosen for this work, of each oxygen carrier sample was analyzed in the particle size analyzer Camsizer XT and visualized in Fig. 5 as cumulative size distribution charts. Sand is also included in each graph as reference.

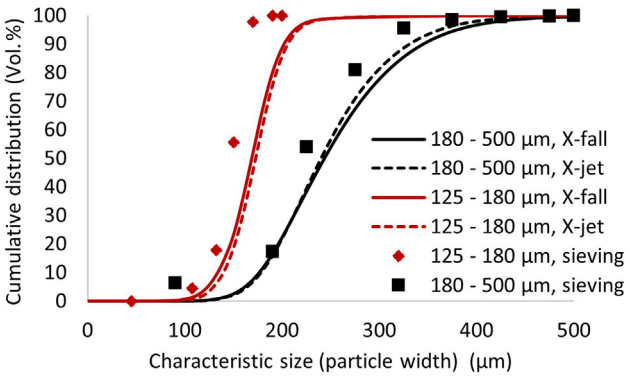

Fig. 3. Comparison between X-fall and X-jet dispersion methods for particle size analysis of ILFC.

The cumulative distribution percentage obtained from the analysis is expressed in volume percentage. This is deemed suitable to visualize a representative particle size distribution according to ISO 9276-1:1998 (Pei et al., 2021).

Fig. 5 shows that the particle size distribution of ilmenite ore and iron sand is generally stable and similar to that of sand independent of mass conversion degree. The only difference is that the freshly calcined ilmenite ore is slightly coarser than the other ilmenite ore samples, while this is not the case with iron sand. In fact, ISSR is slightly coarser than the other iron sand samples. Their particle size range also agrees with the original size range obtained from sieving, i.e., 125–180 μm. We have previously seen that both ilmenite and iron sand show a good attrition resistance at different mass conversion degrees (Purnomo et al., 2024), so it is reasonable that they have quite a consistent particle size independent of mass conversion degrees.

All synthetic ilmenite and LD slag samples are finer than sand, with LD slag presents the highest amount of fine particles with wide distribution. Their freshly calcined samples, SIFC and LDFC, have the coarsest size distribution, with the latter one presenting the highest share of particles above 180 μm. This is in line with previous studies reporting that both materials, i.e., synthetic ilmenite and LD slag, may break easily into smaller fragments (Hildor et al., 2019; Purnomo et al., 2024). Furthermore, LD slag gives the highest deviation from the original sieving range. This is not necessarily caused by the inadequacy of the particle size and shape analysis method used in this work, but rather due to the intrinsic traits of the material itself which can break easily into fines due to its heterogeneous composition (Rydén et al., 2018). This can cause the formation of satellite particles, which tend to easily stick to the wall, demonstrating that the particles' physical properties have been changed. Thus, LD slag should be treated as a special case for this purpose. Freshly calcined mill scale (MSFC) is finer than the other mill scale samples, which is a unique trend only observed in mill scale. The other mill scale samples show similar particle size distributions to that of sand.

The results above can be further broken down into particle width at different cumulative distributions in Fig. 6. Here, the particle width of oxygen carrier particles at cumulative distributions of 10, 50, and 90 vol% are presented altogether with their respective standard deviation, which is presented as error bars, from 2 to 3 repetitions.

As mentioned above, Fig. 6 demonstrates once more that the particle size distributions of ilmenite ore and iron sand remain relatively stable independent of mass conversion degree and seem similar to that of sand. SIFC and SIMR are the coarsest and the finest, respectively, among all synthetic ilmenite samples. In the case of LD slag, LDFC is the coarsest, yet LDFO seems to be the finest. As suggested above, MSFC is clearly the finest mill scale sample, which presents a different behavior from the previous samples. Overall, the data reliability is high.

In contrast to our initial hypothesis, mass conversion degree apparently only influences the particle size distribution of the activated oxygen carrier materials to a minor extent. These include those who were exposed to redox cycles in fluidized bed, i.e., fully oxidized, moderately reduced, and substantially reduced samples. Nevertheless, the contrast is prominent when comparing the freshly calcined to the activated materials. While ilmenite ore and iron sand are the least affected, there is still a small difference on the particle size distribution of their freshly calcined and activated forms. A clear difference is presented for the freshly calcined forms of synthetic ilmenite and LD slag, which are coarser than their respective activated samples, while mill scale shows the opposite phenomenon.

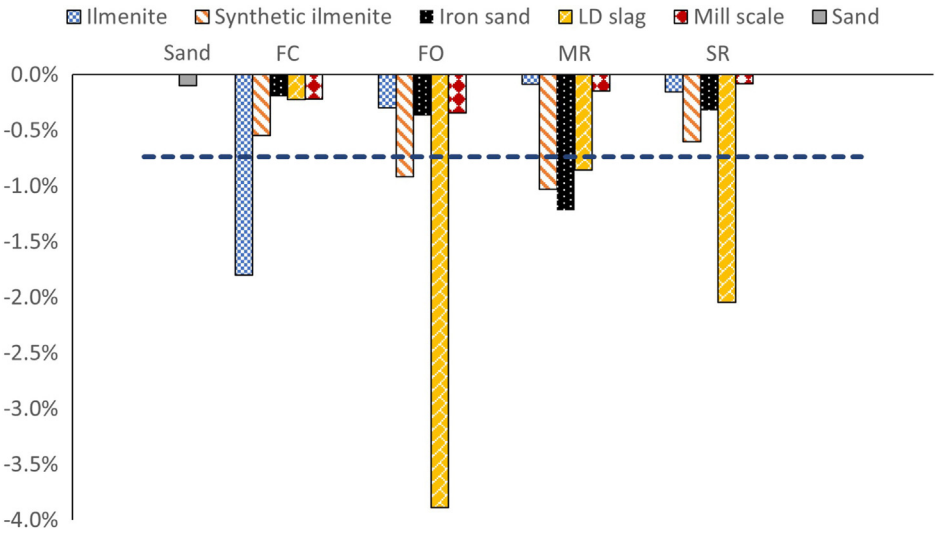

Fig. 4. Weight loss of each oxygen carrier sample during the particle size and shape analysis using X-fall dispersion method. The average value is indicated by the dashed line.

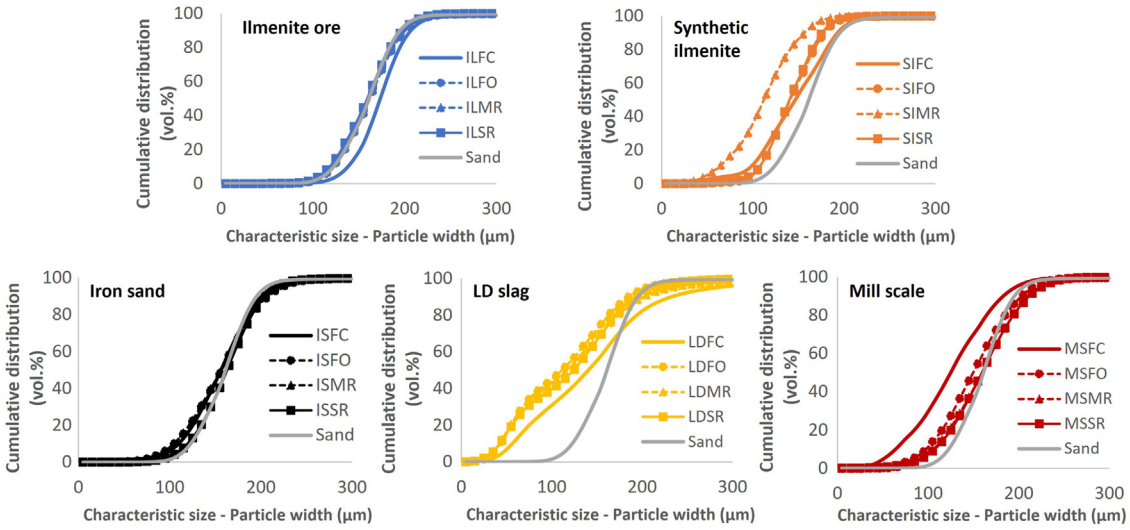

Fig. 5. Volume-weighted particle size distributions of the investigated oxygen carriers and sand.

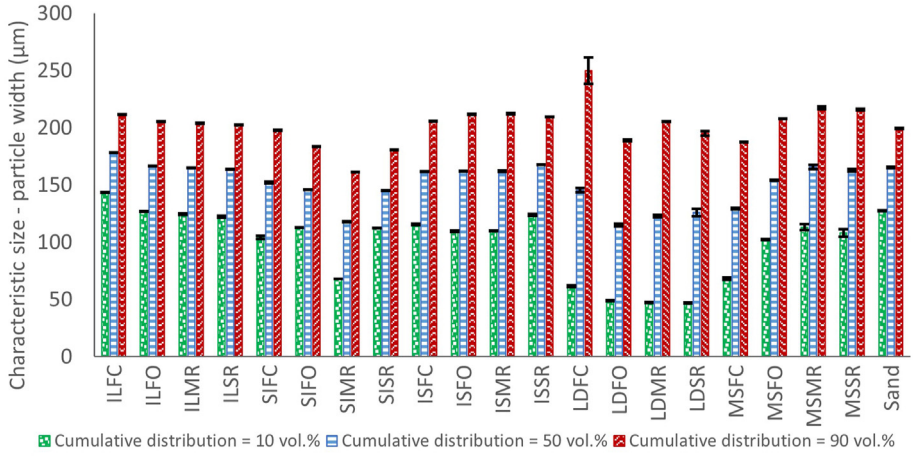

Fig. 6. Particle width of oxygen carriers at cumulative distributions of 10, 50, and 90 vol%.

3.3. Particle shape properties at different mass conversion degrees

The sphericity and aspect ratio of the oxygen carrier samples was analyzed in the particle size analyzer Camsizer XT and visualized in Fig. 7 against the particle characteristic size. Sand is also included in every graph. As a reference, the volume-weighted particle size distribution presented in Fig. 5 is also included. It is important to note that the reference size for the discussion is the original sieving size range, which is 125–180 μm. This is despite the fact that some samples, like all LD slag samples, SIFO, and MSFC, deviate significantly from this size range. The plots are restricted to values between 1 and 99% of the cumulative distribution range.

Within the sieving size range, sand particles present a sphericity varying from 0.85, for the fine particles, to 0.88 for the coarse particles. The sphericity trend of ilmenite ore, ranging between 0.82 and 0.88, closely follows that of sand independent of mass conversion degree. The same pattern and range can also be seen in the case of iron sand, despite being within a slightly lower range, i.e., between 0.79 and 0.83. Note that the decreasing sphericity trend of ISFC at particle widths lower than 100 μm represents only less than 10 vol% of the sample bulk. Synthetic ilmenite shows the highest values of sphericity at around 0.88 in most cases, except those of SIMR which range from 0.83 to 0.86. LD slag shows a rather stable sphericity at around 0.83. However, this is not the case with LDFC, which shows an increasing sphericity trend from 0.74 to 0.80. Mill scale has an increasing trend with sphericity from 0.81 to 0.84 within the sieving size range. Freshly calcined mill scale (MSFC), which has been found to be the finest mill scale sample, shows an increasing sphericity trend from around 0.63 to 0.77 at particle widths below 100 μm, which represents nearly 30 vol% of the sample bulk.

Tables 5 and 6 present the average sphericity and aspect ratio of all oxygen carrier samples, with values in brackets representing that of the particles within the original sieving range. Table 5 clearly shows that average sphericity of the oxygen carriers from both within and outside the original sieving size range are similar. In general, a sphericity of 0.78–0.86 can be assumed for oxygen carrier materials for practical applications. This aligns with a previous study by Schwebel et al. (Schwebel et al., 2014) which assumed the sphericity of an ilmenite ore at the same size range to be 0.79. On the other hand, Table 6 shows that, in most cases, similar aspect ratios can be expected in both the sieving range (125–180 μm) and all the detected size ranges. The aspect ratios of oxygen carriers generally lie between 0.65 and 0.73, with mill scale and synthetic ilmenite being the most and least elongated, respectively. The former also shows the highest difference on the aspect ratio between within the sieving range and all the detected size ranges, see its average values in Table 6.

All in all, contrary to our initial conjecture, mass conversion degree alone seems to have an insignificant effect on both sphericity and the aspect ratio of the particles. According to Blott and Pye (2008), the oxygen carrier materials presented have a high sphericity and slightly elongated particles.

3.4. Crystalline phases of oxygen carriers

Different mass conversion degrees mean different crystalline phases. The crystalline phases of the oxygen carriers are presented in Table 7 to illustrate the phase transformation taking place in oxygen carrier materials.

The phase transformation data clearly shows that the crystalline phases of freshly calcined and fully oxidized oxygen carriers are always identical in this study. However, the biggest differences in particle width and, to a lesser extent, shape, were found between freshly calcined and fully oxidized oxygen carriers of the same materials. This demonstrates that the particle size and shape do change during fluidization. Based on the discussion in sub-section 3.3, such a change is more apparent on some materials, such as synthetic ilmenite, LD slag, and mill scale. The same data also reveals that different mass conversion degree of the activated materials means different crystalline phases, yet the particle width of these materials is usually almost similar. This suggests that, contrary to our initial conjecture, crystalline phases barely have any influence on the particle width of oxygen carriers.

However, at higher oxidation states, the higher content of oxygen in the crystal structures is reportedly associated with a volume increase of the unit cells of around 15–25 vol% (see Tables 8 and 9). As this change in volume was not observed with

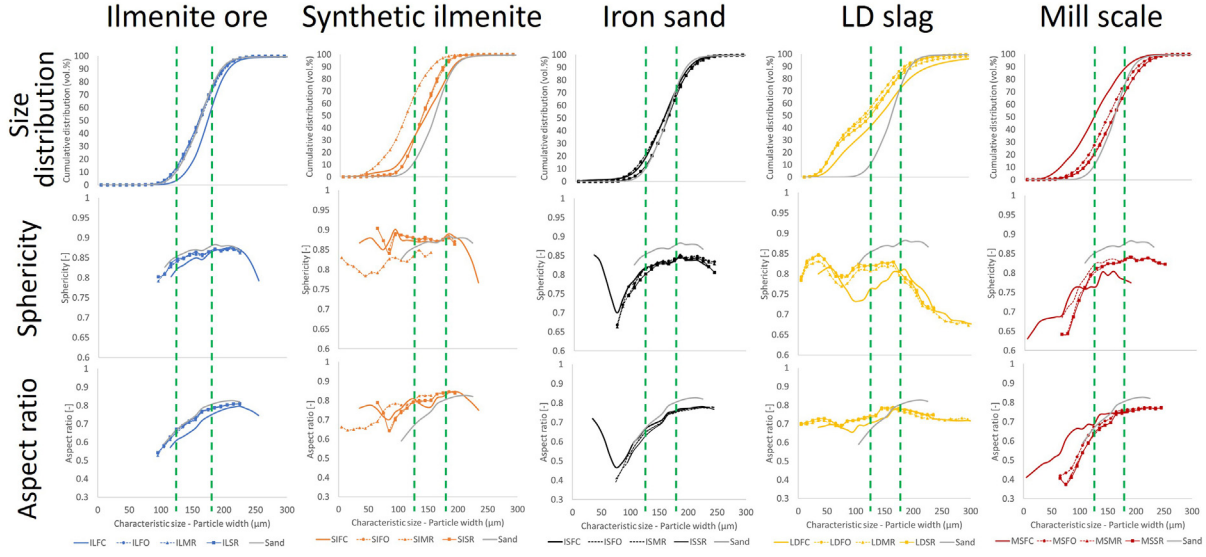

Fig. 7. Measured sphericity and aspect ratio of all oxygen carrier samples and sand plotted against characteristic size. The green dashed lines indicate the original sieving size range (125–180 μm).

Table 5
Average sphericity of oxygen carrier samples from all detected size ranges and the original sieving size range (in brackets).

Oxygen carrier	Freshly calcined (FC)	Fully oxidized (FO)	Moderately reduced (MR)	Substantially reduced (SR)	Average values
Ilmenite ore (IL)	0.85 (0.84)	0.86 (0.86)	0.86 (0.85)	0.86 (0.86)	0.86 (0.85)
Synthetic ilmenite (SI)	0.86 (0.87)	0.88 (0.88)	0.83 (0.83)	0.88 (0.88)	0.86 (0.86)
Iron sand (IS)	0.83 (0.83)	0.84 (0.83)	0.83 (0.83)	0.84 (0.82)	0.83 (0.83)
LD slag (LD)	0.76 (0.78)	0.79 (0.82)	0.78 (0.81)	0.79 (0.82)	0.78 (0.81)
Mill scale (MS)	0.78 (0.77)	0.83 (0.83)	0.82 (0.82)	0.83 (0.82)	0.81 (0.81)

Table 6
Average aspect ratio of oxygen carrier samples from all detected size ranges and the original sieving size range (in brackets).

Oxygen carrier	Freshly calcined (FC)	Fully oxidized (FO)	Moderately reduced (MR)	Substantially reduced (SR)	Average values
Ilmenite ore (IL)	0.72 (0.67)	0.73 (0.72)	0.72 (0.72)	0.72 (0.72)	0.72 (0.71)
Synthetic ilmenite (SI)	0.78 (0.81)	0.78 (0.79)	0.74 (0.79)	0.78 (0.81)	0.77 (0.80)
Iron sand (IS)	0.67 (0.71)	0.68 (0.69)	0.67 (0.69)	0.69 (0.69)	0.68 (0.69)
LD slag (LD)	0.72 (0.74)	0.74 (0.75)	0.73 (0.74)	0.74 (0.75)	0.73 (0.75)
Mill scale (MS)	0.62 (0.69)	0.66 (0.72)	0.66 (0.69)	0.65 (0.69)	0.65 (0.70)

Table 7
Crystalline phases of oxygen carrier samples observed by XRD.

Oxygen carrier	Mass conversion degree	Sample code	Crystalline phases
Ilmenite ore	1.00 (freshly calcined)	ILFC	Fe_2TiO_5, Fe_2O_3, TiO_2
	1.00 (fully oxidized)	ILFO	Fe_2TiO_5, Fe_2O_3, TiO_2
	0.99	ILMR	Fe_2TiO_5, $FeTiO_3$, TiO_2
	0.98	ILSR	Fe_2TiO_5, Fe_2O_3, Fe_3O_4, TiO_2
Synthetic ilmenite	1.00 (freshly calcined)	SIFC	Fe_2TiO_5, Fe_2O_3, TiO_2
	1.00 (fully oxidized)	SIFO	Fe_2TiO_5, Fe_2O_3, TiO_2
	0.99	SIMR	Fe_2TiO_5, $FeTiO_3$, TiO_2
	0.98	SISR	Fe_2TiO_5, $FeTiO_3$, TiO_2
Iron sand	1.00 (freshly calcined)	ISFC	Fe_2O_3, Fe_3O_4, SiO_2
	1.00 (fully oxidized)	ISFO	Fe_2O_3, Fe_3O_4, SiO_2
	0.99	ISMR	Fe_2O_3, Fe_3O_4, Fe_2SiO_4, SiO_2
	0.98	ISSR	Fe_2O_3, Fe_3O_4, FeO, SiO_2
LD slag	1.00 (freshly calcined)	LDFC	Fe_2O_3, Fe_3O_4, $Ca_2Fe_2O_5$, Ca_2SiO_4, CaO
	1.00 (fully oxidized)	LDFO	Fe_2O_3, Fe_3O_4, $Ca_2Fe_2O_5$, Ca_2SiO_4, CaO
	0.99	LDMR	Fe_3O_4, $Fe_{11}O_{12}$, $Ca_2Fe_2O_5$, Ca_2SiO_4, CaO
	0.98	LDSR	Fe_3O_4, $Fe_{1-\delta}O_{12}$, $Ca_2Fe_2O_5$, Ca_2SiO_4, CaO
Mill scale	1.00 (freshly calcined)	MSFC	Fe_2O_3
	1.00 (fully oxidized)	MSFO	Fe_2O_3
	0.96	MSMR	Fe_3O_4, FeO
	0.91	MSSR	Fe_3O_4, FeO, $Fe_{1-\delta}O$, Fe

any of the methods employed, it can be speculated that the reduction from an oxidized state is likely associated with pore formation. The largest theoretical volume increase occurs during the oxidation of Fe to FeO, followed by FeO to Fe_3O_4. These reactions likely occur during the oxidation of reduced iron mill scale which could be the explanation of the unique behavior of this material, i.e., its activated forms being coarser than its freshly calcined counterpart.

3.5. Influence of redox cycles on particle size and shape

Based on the discussion above, it seems that whether the material was exposed to redox cycles or not may have more effect on the particle size and shape of some materials. Table 10 summarizes the classifications of both freshly calcined and fully oxidized particles published by Blott and Pye (2008) within the sieving range (125–180 μm) in three different particle size and shape aspects,

Table 8
Volume per formula unit for different iron oxides in the materials.

Iron oxide phase	Volume per unit cell (Å^3)	Formula units per unit cell	Volume per formula unit (Å^3)
Fe_2O_3	301.2	6	50.2
Fe_3O_4	590.8	8	73.85
FeO	79.29	4	19.82
$FeTiO_3$	315.8	6	52.64
Fe_2TiO_5	364.7	4	91.18
TiO_2	62.4	2	31.22
Fe_2SiO_4	301.6	4	75.39
SiO_2	113	3	37.67
Fe	23.55	2	11.78

Table 9
Theoretical volume increases during oxidations of different iron oxides in the materials.

Reaction	Volume in reduced form (Å^3)	Volume in oxidized form (Å^3)	Volume increase (vol%)
$2\ FeTiO_3 + 0.5\ O_2 \rightarrow Fe_2TiO_5 + TiO_2$	105.3	122.4	16.3
$2\ Fe_3O_4 + 0.5\ O_2 \rightarrow 3\ Fe_2O_3$	147.7	150.6	2.0
$3\ FeO + 0.5\ O_2 \rightarrow Fe_3O_4$	59.47	73.85	24.2
$Fe_2SiO_4 + 0.5\ O_2 \rightarrow Fe_2O_3 + SiO_2$	75.39	87.87	16.5
$Fe + 0.5\ O_2 \rightarrow FeO$	11.78	19.82	68.3

Table 10
Classifications for freshly calcined and fully oxidized oxygen carriers in terms of particle size and shape aspects based on terms published by Blott and Pye (2008).

Oxygen carrier	Freshly calcined	Fully oxidized
Ilmenite ore (IL)	Highly circular, slightly elongate	Highly circular, slightly elongate
Synthetic ilmenite (SI)	Highly circular, not elongate	Highly circular, slightly elongate
Iron sand (IS)	Highly circular, slightly elongate	Highly circular, slightly elongate
LD slag (LD)	Moderately circular, slightly elongate	Highly circular, slightly elongate
Mill scale (MS)	Moderately circular, slightly elongate	Highly circular, slightly elongate

which are extracted as average values from Figs. 4–6. Further, the SEM images of freshly calcined and fully oxidized iron sand and mill scale are also provided in Fig. 8 as an illustration.

Among the examined materials, the influence of exposure to redox cycles in the fluidized bed seems to have the least observable influence on ilmenite ore and iron sand, both being the most robust materials in terms of their attrition resistance (Purnomo et al., 2024). In the case of synthetic ilmenite, LD slag, and mill scale, exposure to multiple redox cycles in the batch fluidized bed seems to have altered their sphericity or aspect ratio to some extents. Fig. 8 shows how the iron sand particles look similar after exposure to redox cycles in the fluidized bed batch reactor, while a few of the mill scale particles seem to become more rounded. It should be noted that the suggested classification systems cover quite broad ranges of sphericity and aspect ratio, so the observable changes in the categories may imply significant figures. This suggests that an exposure to redox cycles in fluidized bed reactor can alter the particle size distribution of iron-based oxygen carriers depending on the type of the materials.

3.6. Implications to practical processes

The results demonstrate that the particle size and shape analysis of DIA method using the standard ISO 13322-2:2021 (International

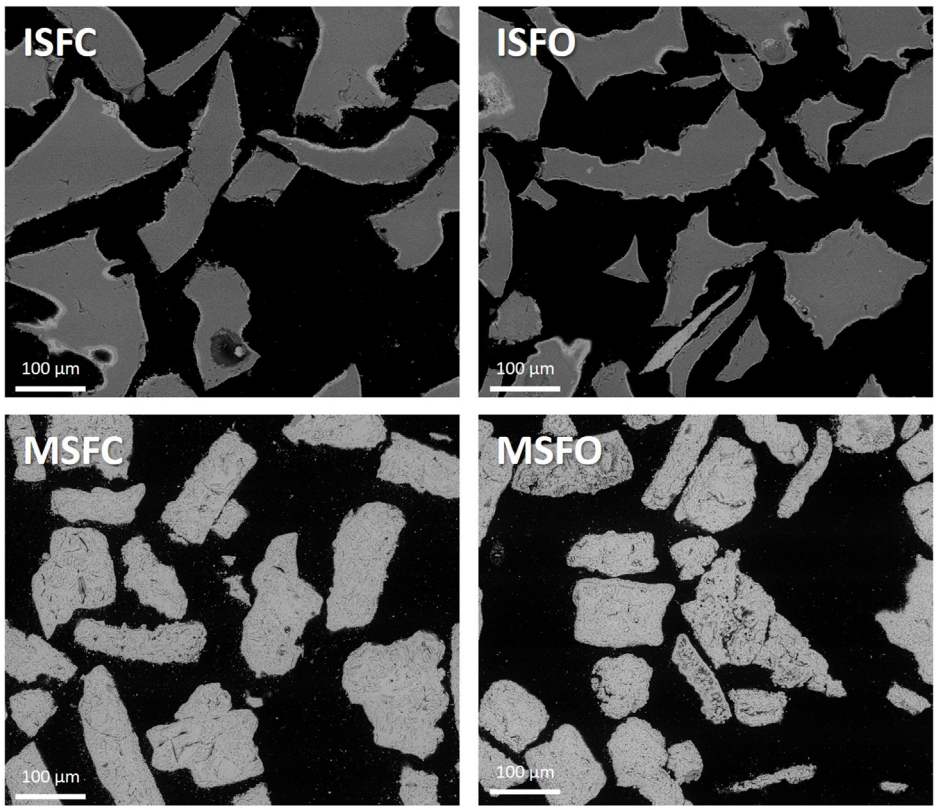

Fig. 8. SEM images of freshly calcined iron sand (ISFC), fully oxidized iron sand (ISFO), fresh calcined mill scale (MSFC), and fully oxidized mill scale (MSFO).

Organization for Standardization, 2021) was able to successfully investigate the particle size distribution, sphericity, and aspect ratio of different iron-based oxygen carriers at multiple oxidation states. Considering that this method works with as little as few grams sample, this can be regarded as a clear benefit as opposed to conventional method of analyzing the particle size distribution of oxygen carriers using manual sieving. This method can therefore be endorsed to examine the particle size and even shape properties of oxygen carriers in both laboratory and industrial settings, e.g., in a commercial OCAC unit.

In a larger reactor system with high gas velocities, the attrition rate is expected to be higher and will influence both the size and shape of the particles. The activation of the oxygen carriers was in this study done in a small, fluidized bed reactor with low gas velocities. Any size change due to attrition in this work is therefore unlikely, which is confirmed by the fact that the calcined samples have a similar size range as the activated samples. While the oxidation state, i.e., mass conversion degree, of an oxygen carrier seem to have a negligible influence on its particle size and shape, exposures to redox cycles in any reactor, including OCAC and chemical looping, can alter its particle size distribution. This implies that the density data obtained for a freshly calcined material may not necessarily be valid for a used material. In many cases, the particle size and shape of oxygen carriers tend to change after being exposed to multiple redox cycles. Therefore, it would be useful to reanalyze the density of used oxygen carriers from any continuous process from time to time as this might give a simple useful indication of the oxygen carriers' lifetime.

4. Conclusion

Particle size and shape analysis using dynamic analysis method (DIA) has been successfully performed on five different iron-based oxygen carriers. It is clear that this method is able to examine the particle size distribution, sphericity, and aspect ratio of oxygen carriers in an accurate and efficient manner compared to the conventional methods, e.g., manual mechanical sieving. Contrary to our initial hypothesis, mass conversion degree of oxygen carriers only affected their particle size and shape to a minor extent. Nevertheless, exposures to multiple redox cycles in fluidized bed reactors may alter the particle size and shape of oxygen carriers substantially. With respect to such an exposure, synthetic ilmenite, LD slag and mill scale are moderately affected, while ilmenite ore and iron sand tend to show stable size distribution and shape properties.

Declaration of interests

The authors declare that they have no known competing financial interests or personal relationships that could have appeared to influence the work reported in this article.

Acknowledgments

This work is a part of the project EU CLARA (Chemical Looping Gasification for Sustainable Production of Biofuels), which has received funding from the European Union's Horizon 2020 research and innovation program under grant agreement No 817841. This study has also received fundings from the Swedish Energy Agency (Project 51430-1) and Stiftelsen ÅForsk (Project 20-269). Boliden AB is acknowledged for iron sand sourcing. The authors would like to thank Bio4Energy, a Strategic Research Environment appointed by the Swedish government.

References

Abián, M., Abad, A., Izquierdo, M. T., Gayán, P., de Diego, L. F., García-Labiano, F., & Adánez, J. (2017). Evaluation of (Mn_xFe_{1-x})$2Ti_yO_z$ particles as oxygen carrier for chemical looping combustion. *Energy Procedia, 114*, 302–308. https://doi.org/10.1016/j.egypro.2017.03.1171

Adánez, J., Cuadrat, A., Abad, A., Gayán, P., Diego, L. F. D., & García-Labiano, F. (2010). Ilmenite activation during consecutive redox cycles in chemical-looping combustion. *Energy and Fuels, 24*(2), 1402–1413. https://doi.org/10.1021/ef900856d

Adánez, J., De Diego, L. F., García-Labiano, F., Gayán, P., Abad, A., & Palacios, J. M. (2004). Selection of oxygen carriers for chemical-looping combustion. *Energy and Fuels, 18*(2), 371–377. https://doi.org/10.1021/ef0301452

Askaripour, M. (2018). *Improving the reactivity of ilmenite as an oxygen carrier in chemical looping combustion*. https://dam-oclc.bac-lac.gc.ca/download?is_thesis=1&oclc_number=1132097800&id=357848b9-f8a2-4be3-a781-96367d71ae37&fileName=34835.pdf.

Blott, S. J., & Pye, K. (2008). Particle shape: A review and new methods of characterization and classification. *Sedimentology, 55*(1), 31–63. https://doi.org/10.1111/j.1365-3091.2007.00892.x

Cho, P., Mattisson, T., & Lyngfelt, A. (2004). Comparison of iron-, nickel-, copper- and manganese-based oxygen carriers for chemical-looping combustion. *Fuel, 83*(9), 1215–1225. https://doi.org/10.1016/j.fuel.2003.11.013

Cuadrat, A., Abad, A., Adánez, J., De Diego, L. F., García-Labiano, F., & Gayán, P. (2012). Behavior of ilmenite as oxygen carrier in chemical-looping combustion. *Fuel Processing Technology, 94*(1), 101–112. https://doi.org/10.1016/j.fuproc.2011.10.020

De Vos, Y., Jacobs, M., Van Der Voort, P., Van Driessche, I., Snijkers, F., & Verberckmoes, A. (2020). Development of stable oxygen carrier materials for chemical looping processes—A review. *Catalysts, 10*(8). https://doi.org/10.3390/catal10080926

Ding, N., Zhang, P., Guan, N., Jiang, G., Zhang, C., & Liu, Z. (2018). Effect of lime addition to CASO4 oxygen carrier in chemical looping combustion. *Brazilian Journal of Chemical Engineering, 35*(1), 155–167. https://doi.org/10.1590/0104-6632.20180351s20160299

Eggers, T., Rackl, H., & von Lacroix, F. (2023). Investigation of the influence of the mixing process on the powder characteristics for cyclic reuse in selective laser sintering. *Powders, 2*(1), 32–46. https://doi.org/10.3390/powders2010003

Eppala, V. C. R., Varghese, M. M., & Vakamalla, T. R. (2023). Effect of particle shape on the hydrodynamics of gas-solid fluidized bed. *Chemical Engineering Research and Design, 189*, 461–473. https://doi.org/10.1016/j.cherd.2022.11.025

Faust, R., Valizadeh, A., Qiu, R., Tormachen, A., Maric, J., Vilches, T. B., Skoglund, N., Seemann, M., Halvarsson, M., Öhman, M., & Knutsson, P. (2023). Role of surface morphology on bed material activation during indirect gasification of wood. *Fuel, 333*. https://doi.org/10.1016/j.fuel.2022.126387

Hildor, F., Leion, H., & Mattisson, T. (2022). Steel converter slag as an oxygen carrier—Interaction with sulfur dioxide. *Energies, 15*(16), 1–29. https://doi.org/10.3390/en15165922

Hildor, F., Mattisson, T., Leion, H., Linderholm, C., & Rydén, M. (2019). Steel converter slag as an oxygen carrier in a 12 MWth CFB boiler – Ash interaction and material evolution. *International Journal of Greenhouse Gas Control, 88*, 321–331. https://doi.org/10.1016/j.ijggc.2019.06.019

Hilton, J. E., Mason, L. R., & Cleary, P. W. (2010). Dynamics of gas-solid fluidised beds with non-spherical particle geometry. *Chemical Engineering Science, 65*(5), 1584–1596. https://doi.org/10.1016/j.ces.2009.10.028

International Organization for Standardization. (2021). *Particle size analysis — Image analysis methods — Part 2: Dynamic image analysis methods*. ISO 13322-2:2021.

Khan, M. N., Chiesa, P., Cloete, S., & Amini, S. (2020). Integration of chemical looping combustion for cost-effective CO2 capture from state-of-the-art natural gas combined cycles. *Energy Conversion and Management: X, 7*, Article 100044. https://doi.org/10.1016/j.ecmx.2020.100044

Leion, H., Frick, V., & Hildor, F. (2018). Experimental method and setup for laboratory fluidized bed reactor testing. *Energies, 11*(10). https://doi.org/10.3390/en11102505

Li, L., & Iskander, M. (2021). Comparison of 2D and 3D dynamic image analysis for characterization of natural sands. *Engineering Geology, 290*, Article 106052. https://doi.org/10.1016/j.enggeo.2021.106052

Lunewski, J., & Schmidt, E. (2023). Experimental investigation into paper dust formation during knife edge cutting on a laboratory scale. *Nordic Pulp & Paper Research Journal, 38*(1), 59–72. https://doi.org/10.1515/npprj-2022-0070

Luo, S., Zeng, L., & Fan, L. S. (2015). Chemical looping technology: Oxygen carrier characteristics. *Annual Review of Chemical and Biomolecular Engineering, 6*, 53–75. https://doi.org/10.1146/annurev-chembioeng-060713-040334

Lyngfelt, A. (2011). Transporteurs d'oxygène pour la combustion en boucle chimique: Experience accumulée pendant 4000 h d'opération. *Oil & Gas Science and Technology, 66*(2), 161–172. https://doi.org/10.2516/ogst/2010038

Ma, J., Han, D., & Zhao, H. (2022). Investigation on iron ore for the oxygen carrier aided combustion. *Fuel Processing Technology, 230*, Article 107214. https://doi.org/10.1016/j.fuproc.2022.107214

Marx, F., Dieringer, P., Ströhle, J., & Epple, B. (2021). Design of a 1 MWth pilot plant for chemical looping gasification of biogenic residues. *Energies, 14*(9), 1–25. https://doi.org/10.3390/en14092581

Mattisson, T., Adánez, J., Mayer, K., Snijkers, F., Williams, G., Wesker, E., Bertsch, O., & Lyngfelt, A. (2014). Innovative oxygen carriers uplifting chemical-looping

combustion,Chemical-looping combustion, natural gas, integrated project, oxygen carrier development. *Energy Procedia, 63*, 113–130. https://doi.org/10.1016/j.egypro.2014.11.012

Mema, I., Wagner, E. C., van Ommen, J. R., & Padding, J. T. (2020). Fluidization of spherical versus elongated particles - experimental investigation using X-ray tomography. *Chemical Engineering Journal, 397*, 125203. https://doi.org/10.1016/j.cej.2020.125203

Ocanha, E. S., Zinani, F. S. F., Modolo, R. C. E., & Santos, F. A. (2020). Assesment of the effects of chemical and physical parameters in the fluidization of biomass and sand binary mixtures through statistical analysis. *Energy, 190*. https://doi.org/10.1016/j.energy.2019.116401

Pei, Y., Hinchliffe, B. A., & Minelli, C. (2021). Measurement of the size distribution of multimodal colloidal systems by laser diffraction. *ACS Omega, 6*(22), 14049–14058. https://doi.org/10.1021/acsomega.1c00411

Purnomo, V., Faust, R., Ejjeta, L. A., Mattisson, T., & Leion, H. (2024). *Effect of oxidation degree of iron-based oxygen carriers on their mechanical strength* (submitted for publication).

Purnomo, V., Hildor, F., Knutsson, P., & Leion, H. (2023). Interactions between potassium ashes and oxygen carriers based on natural and waste materials at different initial oxidation states. *Greenhouse Gases: Science and Technology, 534*, 520–534. https://doi.org/10.1002/ghg.2208

Purnomo, V., Yilmaz, D., Leion, H., & Mattisson, T. (2021). Study of defluidization of iron- and manganese-based oxygen carriers under highly reducing conditions in a lab-scale fluidized-bed batch reactor. *Fuel Processing Technology, 219*, 106874. https://doi.org/10.1016/j.fuproc.2021.106874

Qasim, M., Ayoub, M., Ghazali, N. A., Aqsha, A., & Ameen, M. (2021). Recent advances and development of various oxygen carriers for the chemical looping combustion process: A review. *Industrial & Engineering Chemistry Research, 60*(24), 8621–8641. https://doi.org/10.1021/acs.iecr.1c01111

Rydén, M., Hanning, M., & Lind, F. (2018). Oxygen Carrier Aided Combustion (OCAC) of wood chips in a 12 MWth circulating fluidized bed boiler using steel converter slag as bed material. *Applied Sciences, 8*(12). https://doi.org/10.3390/app8122657

Ryden, M., Kallen, M., Jing, D., Hedayati, A., Mattisson, T., & Lyngfelt, A. (2014). (Fe1-xMnx)TiyO3 based oxygen carriers for chemical-looping combustion and chemical-looping with oxygen uncoupling. *Energy Procedia, 51*, 85–98. https://doi.org/10.1016/j.egypro.2014.07.010

Ryu, H. J., Bae, D. H., & Jin, G. T. (2003). Effect of temperature on reduction reactivity of oxygen carrier particles in a fixed bed chemical-looping combustor. *Korean Journal of Chemical Engineering, 20*(5), 960–966. https://doi.org/10.1007/BF02697306

Schwebel, G. L., Sundqvist, S., Krumm, W., & Leion, H. (2014). Apparent kinetics derived from fluidized bed experiments for Norwegian ilmenite as oxygen carrier. *Journal of Environmental Chemical Engineering, 2*(2), 1131–1141. https://doi.org/10.1016/j.jece.2014.04.013

Sedor, K. E., Hossain, M. M., & de Lasa, H. I. (2008). Reactivity and stability of Ni/Al2O3 oxygen carrier for chemical-looping combustion (CLC). *Chemical Engineering Science, 63*(11), 2994–3007. https://doi.org/10.1016/j.ces.2008.02.021

Störner, F., Lind, F., & Rydén, M. (2021). Oxygen carrier aided combustion in fluidized bed boilers in Sweden—review and future outlook with respect to affordable bed materials. *Applied Sciences, 11*(17). https://doi.org/10.3390/app11177935

Takehara, M. D. B., García Llamas, Á. D., Chishty, M. A., Umeki, K., & Gebart, R. (2022). Effect of acoustic perturbation on particle dispersion in a swirl-stabilized pulverized fuel burner: Cold-flow conditions. *Fuel Processing Technology, 228*. https://doi.org/10.1016/j.fuproc.2021.107142

Wei, H., Liu, H., Zhao, T., Zhang, S., Ma, L., Yin, M., & Meng, Q. (2022). Particle breakage and morphology changes of calcareous sands under one-dimensional compression loading. *Marine Geophysical Researches, 43*(4), 1–12. https://doi.org/10.1007/s11001-022-09507-8

Yu, Z., Yang, Y., Yang, S., Zhang, Q., Zhao, J., Fang, Y., Hao, X., & Guan, G. (2019). Iron-based oxygen carriers in chemical looping conversions: A review. *Carbon Resources Conversion, 2*(1), 23–34. https://doi.org/10.1016/j.crcon.2018.11.004

Zheng, H., Jiang, X., Gao, Y., Tong, A., & Zeng, L. (2022). *Chemical looping reforming: Process fundamentals and oxygen carriers* (vol. 2 (1)). Springer International Publishing. https://doi.org/10.1007/s43938-022-00012-3

Zornoza, B., Mendiara, T., & Abad, A. (2022). Evaluation of oxygen carriers based on manganese-iron mixed oxides prepared from natural ores or industrial waste products for chemical looping processes. *Fuel Processing Technology, 234*, Article 107313. https://doi.org/10.1016/j.fuproc.2022.107313